Video Article

Reservoir Condition Pore-scale Imaging of Multiple Fluid Phases Using X-ray Microtomography

Matthew Andrew[1], Branko Bijeljic[1], Martin Blunt[1]

[1]Department of Earth Science and Engineering, Imperial College London

Correspondence to: Matthew Andrew at m.andrew11@imperial.ac.uk

URL: https://www.jove.com/video/52440
DOI: doi:10.3791/52440

Keywords: Medicine, Issue 96, Reservoir condition, micro-CT, Multi-phase, Carbon Storage, Capillary Trapping, Pore-scale

Date Published: 2/25/2015

Citation: Andrew, M., Bijeljic, B., Blunt, M. Reservoir Condition Pore-scale Imaging of Multiple Fluid Phases Using X-ray Microtomography. *J. Vis. Exp.* (96), e52440, doi:10.3791/52440 (2015).

Abstract

X-ray microtomography was used to image, at a resolution of 6.6 µm, the pore-scale arrangement of residual carbon dioxide ganglia in the pore-space of a carbonate rock at pressures and temperatures representative of typical formations used for CO_2 storage. Chemical equilibrium between the CO_2, brine and rock phases was maintained using a high pressure high temperature reactor, replicating conditions far away from the injection site. Fluid flow was controlled using high pressure high temperature syringe pumps. To maintain representative *in-situ* conditions within the micro-CT scanner a carbon fiber high pressure micro-CT coreholder was used. Diffusive CO_2 exchange across the confining sleeve from the pore-space of the rock to the confining fluid was prevented by surrounding the core with a triple wrap of aluminum foil. Reconstructed brine contrast was modeled using a polychromatic x-ray source, and brine composition was chosen to maximize the three phase contrast between the two fluids and the rock. Flexible flow lines were used to reduce forces on the sample during image acquisition, potentially causing unwanted sample motion, a major shortcoming in previous techniques. An internal thermocouple, placed directly adjacent to the rock core, coupled with an external flexible heating wrap and a PID controller was used to maintain a constant temperature within the flow cell. Substantial amounts of CO_2 were trapped, with a residual saturation of 0.203 ± 0.013, and the sizes of larger volume ganglia obey power law distributions, consistent with percolation theory.

Video Link

The video component of this article can be found at https://www.jove.com/video/52440/

Introduction

Carbon Capture and Storage is the process where CO_2 is captured from large point sources and stored in porous rock, displacing resident brines so that it remains in the subsurface for hundreds to thousands of years[1]. The CO_2 resides in the subsurface as a dense super-critical phase ($scCO_2$), with properties radically different to CO_2 at ambient conditions. There are four principal mechanisms by which $scCO_2$ might be immobilized in the subsurface: stratigraphic, solubility, mineral and residual trapping. Stratigraphic trapping is where CO_2 is held underneath impermeable seal rocks; solubility trapping is where CO_2 dissolves into the resident brine surrounding the injected CO_2[2-4]; mineral trapping is where carbonate mineral phases are precipitated into the rock[5]; and residual or capillary trapping is where CO_2 is held by surface forces as tiny droplets (ganglia) in the pore-space of the rock[6]. This can occur either naturally, by the migration of the CO_2 plume[7-9], or can be induced by the injection of chase brines[10]. In order to understand the processes governing the flow and trapping of this CO_2 in the subsurface a new suite of experiments must be conducted, harnessing new advances in technology to better understand the fundamental physics associated with multi-phase flow.

X-ray microtomography has developed as a technique over the past 25 years from early attempts to visualize both dry geological samples[11] and multiple fluid phases[12] to the primary method for the non-invasive imaging of rock cores, both for modeling purposes and for experimental implementation[13-15]. Because microtomography is non-invasive, it has the ability to study systems at representative conditions, which is particularly attractive for the CO_2-brine-rock system, as the multiphase flow behavior of $scCO_2$ is highly dependent on thermo-physical properties, such as interfacial tension and contact angle, which are in turn a strong function of system conditions such as temperature, pressure and salinity[16-18]. In such a complex system, with such an extensive and poorly understood set of inter-dependent variables, experiments using idealized pore structures[19] or analogue fluids[20,21] may not be applicable to flow processes in the subsurface. Imaging multiple fluids at conditions representative of a prospective CO_2 injection formation has, however, remained a challenge[22]. In this study we outline a methodology for the examination of multi-fluid behavior at reservoir conditions, focusing on the examination of capillary trapping[23,24]. This will include the designing of an imaging strategy, the assembly of the fluid cell, the injection strategy and subsequent image processing.

The experimental examination of pore-scale multiphase flow behavior in real rock systems focuses on the imaging of partially saturated rock cores after both non-wetting phase injection (drainage) and wetting phase injection (imbibition). These fluids are injected by connecting the cores to fluid injection pumps using flexible flow lines, while confining the core using a Hassler-type coreholder design[25]. To successfully image the *in-situ* arrangement of $scCO_2$ and brine, a novel and highly sensitive experimental setup was used, primarily focusing on the use of a high resolution x-ray microscope[23,24,26]. The requirements for conducting experiments at elevated temperatures and pressures are very stringent,

and require recent developments in both materials technology and micro-CT facilities. The key requirements that have to be fulfilled are that any core/sample holder needs to be able to withstand high pressure high temperature (HPHT) conditions while remaining sufficiently x-ray transparent to allow for effective imaging. Lab-based instruments impose an additional constraint, as the core-holder must be small enough such that the x-ray source can be placed close to the sample and that sufficiently large geometric x-ray magnification can be achieved such that the pore space is effectively resolved. Although this constraint has been relaxed somewhat with the introduction of secondary optics in newer lab-based micro-CT machines, it has not been completely removed, especially if rapid acquisition times are desired, as higher optical magnifications tend to increase the time required to acquire images.

Experiments with soluble fluids provide an additional challenge when using lengthy acquisition times, as CO_2 will diffuse through the polymeric portions of the experimental assembly, reducing the *in-situ* fluid saturation. All these issues meant that scan times longer than around 2 hr were impractical. In order to keep scan times below this requirement, particularly stringent for lab based sources, the core-holder must be around 1 cm in diameter. A larger coreholder size would have required the detector to be much further from the source to achieve the same geometric magnification, reducing the x-ray flux incident on the detector and therefore increasing required projection exposure times. The flow cell used in these experiments was based on a traditional Hassler cell design, built around a carbon fiber sleeve, with a sleeve design similar to that used by Iglauer *et al.*[27], but with two significant alterations: 1) The carbon fiber composite used in the sleeve manufacture was changed from T700 fibers, with a stiffness of 230 GPa, to M55 fibers, with a stiffness of 550 GPa. This not only reduced the amount of sample movement during tomography acquisition, but also increased the maximum working pressure of the cell from 20 MPa to 50 MPa. 2) The sleeve has been elongated from 212 mm to 262 mm to allow the source and detector to be as close to the sample as possible.

A major experimental shortcoming in the first study to use micro-CT to examine CO_2 at reservoir conditions was the use of metal lines to control the flow to and from the core-holder[27]. As the sample is rotated relative to the pumps, the flow lines also need to be rotated. Stiff flow lines can cause the sample to move, reducing effective image resolution or making some or all of the dataset unusable. To prevent this we replaced all the flow lines close to the rotation stage with flexible polyether ether ketone (PEEK) tubing. These flow lines were flexible, providing very small lateral forces (load) to the core-holder during acquisition. We also attached the flow lines to valves attached to the sample stage, rather than attaching the flow lines to the coreholder. This meant that any existing flow-line load was transmitted directly to the stage, rather than to the sample, reducing the probability of sample motion. A major disadvantage of using the PEEK tubing was that CO_2 was able to slowly diffuse through it, over a timescale of around 24 hr. This meant that CO_2 saturated brine left in the flow lines would gradually desaturate.

Another major experimental shortcoming of previous studies was inaccurate control of temperature. This can impact results in a number of ways. Firstly, temperature is a strong control on both interfacial tension and contact angle[16-18]. Moreover, the solubility of both $scCO_2$ and carbonate rock in brine is also highly temperature dependent[28]. Solubility control is critical, as when $scCO_2$ is injected into a saline carbonate aquifer it will dissolve into the resident brine, forming a highly reactive carbonic acid, which will in turn start to dissolve any calcite present. Any inaccuracy in solubility control can therefore lead to $scCO_2$ dissolution/exsolution or solid dissolution/precipitation.

Previous studies[27] used a heated confining fluid to heat the coreholder; however this was problematic. It has the disadvantages associated with the difficulty of accurately maintaining a constant confining pressure using a recirculating water supply, requiring extra heating baths for that supply. Furthermore, this system only maintains an accurate control of temperature at the point of the heating bath (not at the point of the core holder, and the confining fluid would cool between the water bath and the core holder). It also requires both an inlet and an outlet port for the confining fluid, increasing the number of fluid lines attached to the coreholder and so increasing flow line load.

Instead of using a heated confining fluid, a flexible heating jacket was used to surround the core holder. This very simple heating method resulted in very little coreholder load, and allowed for the precise and accurate heating. An extremely thin polyimide heating film was used, in order to minimize sample size. The construction of this film consists of an etched copper foil element 0.0127 mm thick, encapsulated between two layers of 0.0508 mm polyimide film. The copper elements present in the jacket did not noticeably affect image quality. Temperature was measured using a thermocouple sitting in the confining annulus of the cell. It was positioned on the outside of the confining sleeve, as close as possible to the core, ensuring an accurate, reliable and stable reading of the pore-fluid temperature. The thermocouple and heating film were connected to a custom built Proportional Integral Derivative (PID) controller, and temperatures were controlled within ± 1 °C.

To maintain complete control over inter-phase solubility, and represent conditions present in the aquifer far away from the injection site, prior to injection the brine was equilibrated with $scCO_2$ by vigorously mixing the two fluids together with small particles (1-2 mm) of the host rock in a stirred and heated reactor. All wetted components within this reactor are made of Hastelloy to minimize corrosion. The reactor contains a filtered dip tube to allow for denser fluid to be extracted from the base of the reactor (brine) and less dense fluid to be extracted from the top of the reactor ($scCO_2$). High pressure syringe pumps were used to maintain pressure and control flow in the pore-space of the rock and in the reactor, with a displacement accuracy of 25.4 nl. The experimental apparatus used in this study is shown in **Figure 1**. The ionic salt used for the experiment from which the representative results were drawn was Potassium Iodide (KI), as it has a high atomic weight and so a high x-ray attenuation coefficient, making it an effective contrast agent. Less attenuating salts (such as NaCl) or mixtures could be used, however larger salinities would be required to achieve the same x-ray attenuation.

Protocol

1. Imaging Strategy Design

1. In order to predict the imaging performance of different solute choices for the brine, calculate the x-ray spectrum of the incident x-rays[29-31]. Include the impact of the core-holder, core assembly and confining fluids on x-ray spectrum. An example incident x-ray spectrum using an acceleration voltage of 80 kV and electron current of 87 µA is shown in **Figure 1**.
2. Compare this spectrum to the transmission factors of the sample containing different pore-fluids. Simulate changes in the transmission factor due to changes in the pore-fluid using the Beer-Lambert law, assuming an effective optical length of the species within the sample, and calculated x-ray attenuation coefficients (**Figure 3**)[32]. Determine the overall transmission factor by integrating over all incident x-ray energies.

An example of the resulting effective transmission factors for the rock matrix and pore-space material, and the changes in transmission factors relative to the case when the pore-space is filled with vacuum can be seen in **Table 1**.

3. Choose a brine solute and concentration such that the change in transmission factor associated with brine is approximately half the change in transmission factor associated with the solid. This will maximize three phase contrast in the reconstructed image. Weigh out the required amount of salt (7% (w/w) KI was used for the experiment from which the representative results were taken) and vigorously mix with deionized water.
    1. Alternatively, if a specific brine composition is desired, change the x-ray source acceleration voltage to change the spectrum of the incident x-rays.

2. Assembly of Equipment and Cell

1. Assemble the equipment as shown below in **Figure 2**. Use PEEK flowlines to reduce lateral sample load on the flow cell. Test each connection carefully for any fluid leaks.
    1. Place the brine, of composition decided during steps 1.1-1.3, in the base of the reactor. Wrap the flexible heater around the flow cell.
2. Construct metal end fittings. Remove the thread from the 1/8” end of a 1/16” to 1/8” reducer fitting. Then cut small grooves into the face of the 1/8” end of the fitting to distribute the injected CO_2 over the entire face of the core.
3. Pass the high pressure thermocouple through the metal end parts of the micro-flow cell and seal using ¼” ferrules and nut, so the hot junction of the thermocouple sits adjacent to the inlet face of the core, within the confining annulus of the cell.
4. Drill desired sample into a core 6.5 mm in diameter and 30 mm to 50 mm in length. Grind down the ends of the core flat, to ensure a good connection with the metal end pieces. Wrap this core in aluminum foil then place within a flouro-polymer elastomer sleeve.
    1. Connect the ends of the elastomer sleeve to the metal end fittings. Add another wrap of aluminum foil to the exterior of the elastomer sleeve before placing the hot junction of the thermocouple next to the confining annulus of the cell and adding a final wrap of aluminum foil. This forms the core assembly (**Figure 4**).
5. Assemble the micro-flow cell with the core assembly sealed within it and connect the cell to the stage within the micro-CT enclosure (**Figure 5**) using a clamp mounted on top of the rotational CT stage.

3. System Pressurization

1. Close all valves apart from valve 1, 2 and 3, as defined in **Figure 3**. Load CO_2 from the cylinder into pump 1 and the reactor, then close valve 1. Slowly raise the temperature and pressure within the reactor to that desired for the pore fluid during the experiment.
2. Vigorously mix the reactor for at least 12 hr to ensure all phases are in chemical equilibrium prior to injection.
3. Open valve 14 and load the confining fluid into pump 3. Close valve 14. Open valves 12 and 13. Pressurize the confining annulus of the cell to at least 10% higher than the proposed pore-fluid pressure.
4. Open valve 11. Load brine into pump 2. Close valve 11 and open valves 9, 8 and 6.
    1. Slowly pressurize the pore-space of the rock until it is at the desired pore-fluid pressure, filling the pore-space of the sample with brine that has not been equilibrated with $scCO_2$.
5. Open valve 4. Flush more than 1,000 pore volumes of equilibrated brine through the core by refilling pump 2 at a constant flow rate. Pore volume is found by multiplying the core volume by the porosity found using helium porosimetry.
NOTE: This will miscibly displace the un-equilibrated brine, ensuring 100% initial brine saturation and creating conditions in the core akin to the subsurface conditions in an aquifer at a point slightly ahead of the front of a $scCO_2$ plume.

4. Fluid Flow and Image Acquisition

1. Pass through 10 pore volumes (around 1 ml) of $scCO_2$ through the core at very low flow rates (1.67×10^{-9} m^3/sec), ensuring a low capillary number of around 10^{-6}. Continually take 2D projections in order to accurately measure the total injected volume by observing the point when $scCO_2$ displaces brine in the pore space.
2. Pass through 10 pore volumes (around 1 ml) of equilibrated brine through the core at the same low flow rate, causing $scCO_2$ to become trapped as a residual phase in the pore-space.
3. After steps 4.1 or 4.2, take scans of the sample to image drainage or imbibition respectively. Use a voxel size such that the entire diameter of the core fits within the field of view.
4. Reconstruct the scans using a tomographic reconstruction program. To scan the entire length of the core while retain a small voxel size, reconstruct composite volumes by stitching together multiple overlapping sections, acquired sequentially.
NOTE: Each section required around 400 projections, taking 15-20 min to acquire, so the scanning of an entire composite volume took around 90 min.

5. Image Processing and Segmentation

1. Apply a non-local means edge preserving filter[33,34] to the dataset and correct the images for any beam hardening or softening artifacts created during image reconstruction by modeling these artifacts as radially symmetric Gaussian functions[35].
2. Segment the data (turn the greyscale information into a binary representation of the CO_2 within the image) by the use of a watershed algorithm with a seed generated using a 2D histogram[36], treating the CO_2 as one phase and the brine and the rock together as the other phase.
3. Analyze this segmented image to find both the total number of CO_2 voxels and also the sizes of each connected cluster of residual CO_2.

Representative Results

The results for a single carbonate, Ketton limestone, an oolite from the upper Lincolnshire Limestone Member were analyzed in 3D in order to identify and measure the volume of each unique disconnected ganglion, which was then labeled (**Figure 6**). All processing was conducted within the Avizo Fire 8.0 and ImageJ programs[37].

The segmented partially saturated images were analyzed by counting the number of voxels of residually trapped $scCO_2$ to find the proportion of the rock volume occupied by trapped $scCO_2$ — the capillary trapping capacity. This can then be converted to a residual saturation (S_r) by dividing this value by the porosity as obtained using helium porosimetry. Significant proportions of $scCO_2$ were trapped as a residual saturation, with a residual saturation of 0.203 ± 0.013. This agrees with the results found in previous studies using micro-CT[23]. Larger core-scale studies of residual trapping in this rock type showed a lower residual saturation of 0.137 ± 0.012[38].

The ingress of brine into a $scCO_2$ saturated core is an imbibition process where a wetting fluid (brine) invades each pore, displacing non wetting fluid ($scCO_2$). In a strongly water-wet rock we expect the water to fill areas of the pore space in order of size[39,40], trapping disconnected ganglia in the process called snap-off. This process should be percolation like[41] so predictions can be made about the size distribution of the isolated clusters. The number n of clusters of volume s (measured in voxels) should scale as , where τ is the Fisher exponent[42]. Network modeling has shown that in three-dimensional cubic regular lattices the value of this exponent is around τ=2.189[43]. One natural way of extracting this exponent from real data is to plot the binned quantity, as defined by Dias and Wilkinson[41].

$$N_s = \sum_{s'=s}^{2s-1} n_s \qquad (1)$$

which should scale as:

$$N_s \sim s^{-(\tau-1)} \qquad (2)$$

This is then plotted on a log-log plot as a function of s (**Figure 7**), showing power-law behavior for large ganglia, but an under-representation of smaller ganglia compared to the power law model. The exponent was calculated by excluding ganglia smaller than 10^5 voxels (approximately the start of the power-law behavior) and performing Levenberg-Marquardt regression[44,45] using a least absolute residual robust fitting algorithm[46,47]. This was performed using a commercial software package. The Fisher exponent for this system was 2.287 ± 0.009, close to the theoretical value of 2.189, indicating that imbibition in this system is indeed percolation like. More generally these results confirm conclusions in larger core-flood experiments[38,48,49] that $scCO_2$ acts as the non-wetting phase in carbonates.

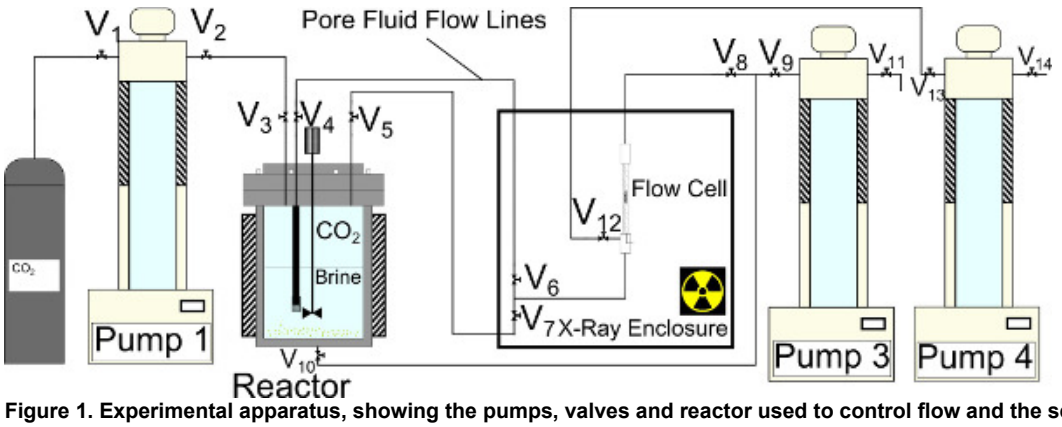

Figure 1. Experimental apparatus, showing the pumps, valves and reactor used to control flow and the seating of the coreholder within the micro-CT enclosure. Please click here to view a larger version of this figure.

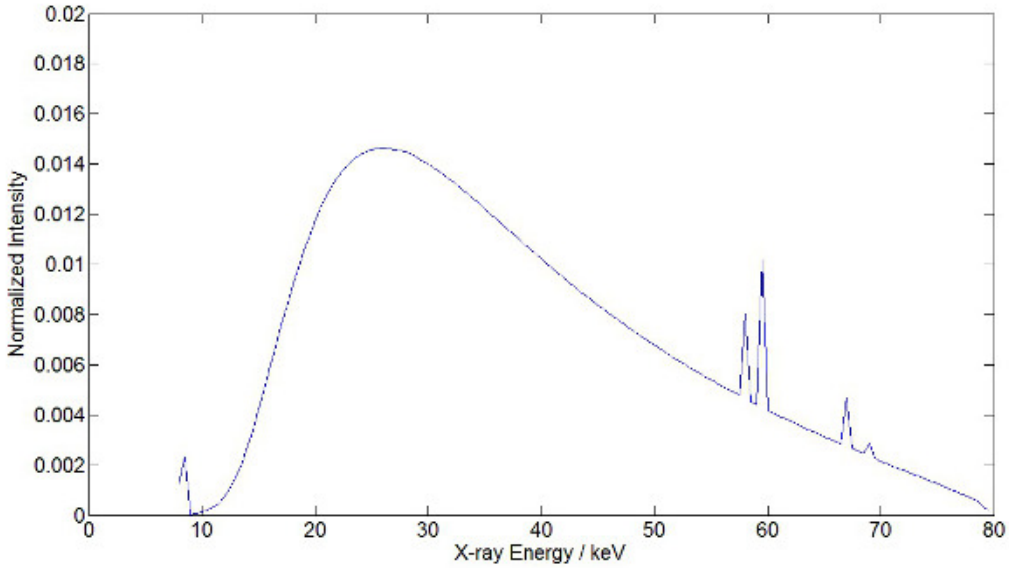

Figure 2. The normalized energy spectrum for x-rays incident on the core, filtered through the coreholder, confining sleeve and confining fluid. Calculated using SpekCALC[29-31].

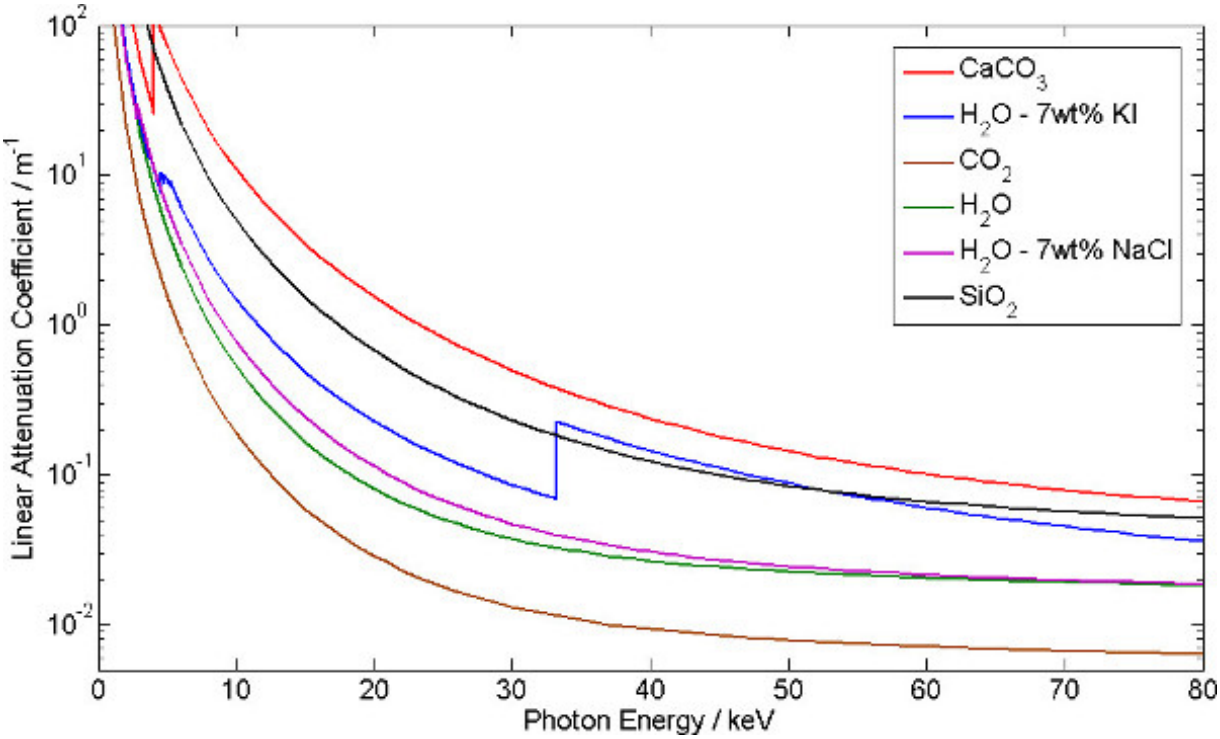

Figure 3. The linear attenuation coefficients of different fluids and rock materials as a function of photon energy.

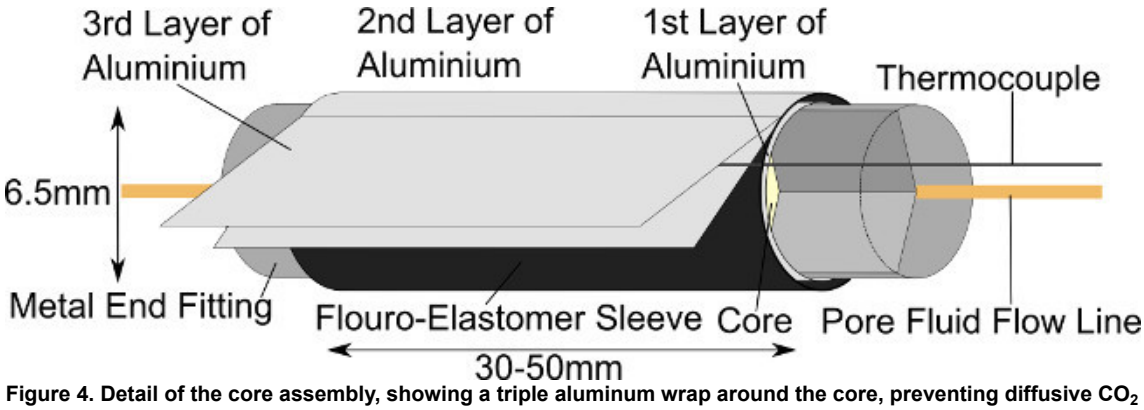

Figure 4. Detail of the core assembly, showing a triple aluminum wrap around the core, preventing diffusive CO_2 exchange across the flouro-elastomer sleeve. Please click here to view a larger version of this figure.

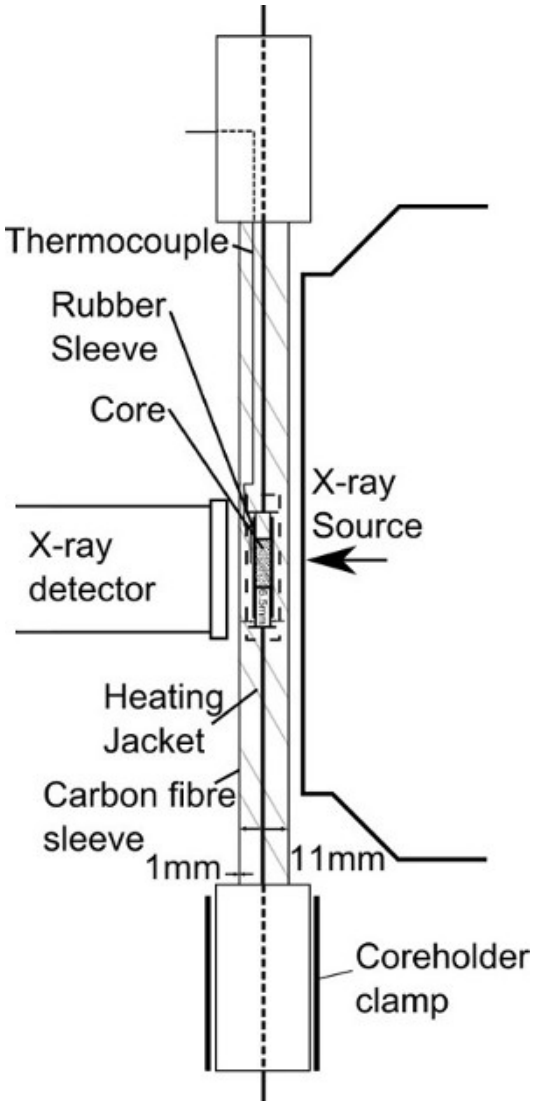

Figure 5. Detail of the flow cell, heating apparatus and siting of the core assembly within the flow cell. The thermocouple must be placed as close as possible to the inlet face of the core. Please click here to view a larger version of this figure.

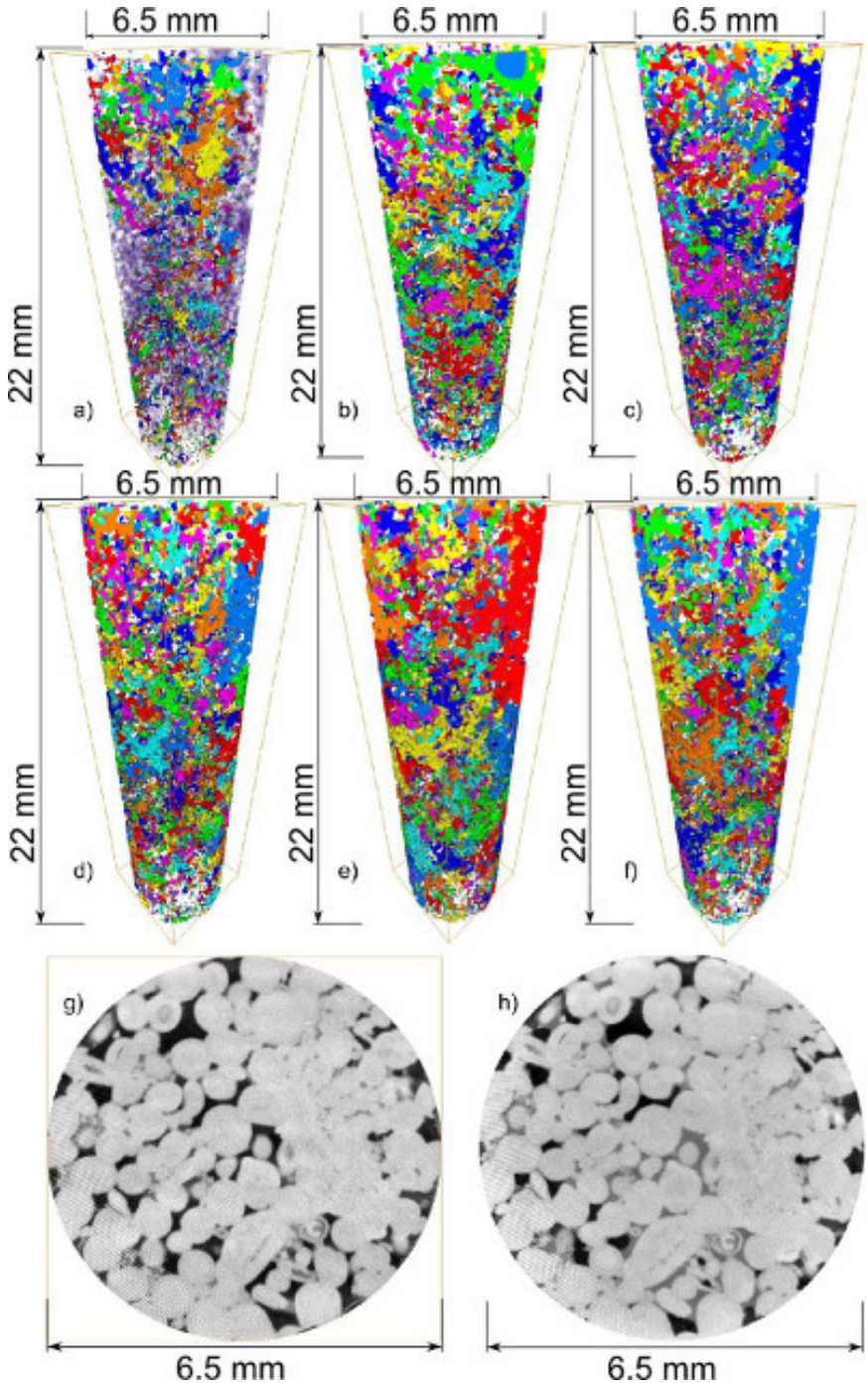

Figure 6. Image of the carbonate after drainage and imbibition. (A) A 3D rendering of the core after drainage where each non-wetting phase cluster is given a different color. **(B-F)** A 3D rendering of the core after five imbibition experiments, colored as described for **(A)**. The large range of colors indicates a poorly connected residual phase. **(G)** A cross-section of the core after drainage. The darkest phase is the $scCO_2$, the intermediate phase is brine and the lightest phase is rock grain. **(H)** A cross-section of the core after imbibition. Please click here to view a larger version of this figure.

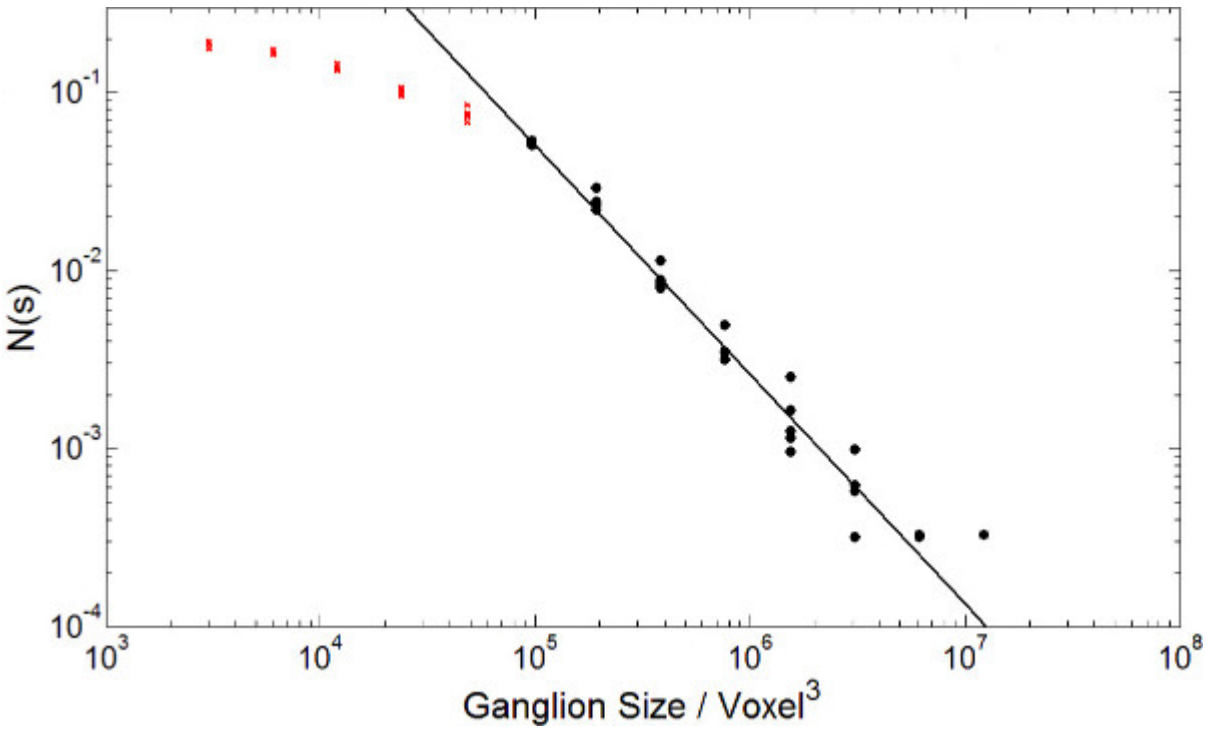

Figure 7. The size distribution of the residual ganglia shown in Figure 6.

Material Filling Porosity	Vacuum	CO_2	H_2O	H_2O – 7 wt% NaCl	H_2O – 7 wt% KI	Solid ($CaCO_3$)
Transmission Factor	0.25	0.247	0.243	0.242	0.224	0.202
Change in transmission factor relative to vacuum	N/A	-0.003	-0.007	-0.008	-0.026	-0.048

Table 1. Summary of results (transmission factor and change in transmission factor relative to the vacuum filled case) from simulation of the x-ray optical properties of the rock and pore-space filling material imaged during this study. Each column represents a different material filling the pore-space of the rock within the coreholder.

Discussion

The most critical steps for successful imaging of multiphase fluids at elevated pressures and temperatures are: 1) The successful isolation of the pore fluid from the surrounding confining fluid; 2) the effective equilibration of the fluids and rock prior to injection; 3) effective temperature control throughout the experiment; and 4) the effective segmentation of the resulting images.

The use of the aluminum wraps is critical for the successful isolation of the pore-fluid from the surrounding confining fluid as in its absence diffusive exchange across the sleeve is rapid, and saturation within the core does not remain constant for the duration of the scan. This problem can also be evident when fluid remains in the PEEK flowlines for extended periods of time (> 2 hr) prior to injection into the core in step 4.1 and 4.2. Once again, CO_2 diffusively exchanges across the plastic, causing the brine to desaturate. If this desaturated brine is injected into the core, the saturation in the core will decrease as residual clusters are dissolved by the injected brine.

Other methods for the equilibration of fluids and rocks, including fluid recirculation[50], have been proposed in the literature. These methods increase the complexity of the experimental setup, which in turn would have increased the amount of time for each experiment, which would have in turn increased the likelihood that the brine in flow lines would have diffusively desaturated.

Effective temperature control is essential, and the presence of a thermocouple within the confining annulus of the flow cell is critical for this. Temperature is only measured at a single point, meaning there may be some gradient across the sample, leading to solubility imbalance and dissolution or exsolution. This can be minimized by locating the hot junction of the thermocouple as close as possible to the inlet face of the rock core.

The effective segmentation of the resulting images can be a real challenge with these systems, as the segmentation of images containing a partial saturation of multiple fluids is significantly more challenging that the segmentation of dry images, so the use of simple grey-scale universal thresholding is insufficient[51]. The use of watershed segmentation not only gives the most reliable results, compared to other algorithms in the literature, but is also the most effective at dealing with ring and partial volume artifacts[35].

One of the most significant limitations of this technique is that it can only access the macro-pore space of a rock. The microporosity (on scales smaller than the image resolution) remains inaccessible, and may be important for multiphase flow. Higher resolutions reveal a greater proportion of these parts of pore space, but also correspond to a decrease in the field of view. The applicability of the technique to a specific rock type could be addressed by comparing the resolution of the scan to the pore throat size distribution obtained using independent method such as mercury injection capillary pressure.

This method is a leading technique for the pore-scale imaging of multiple fluids at reservoir conditions in realistic systems, with existing applications including a cross comparative study of capillary trapping[24] and the measurement of contact angle[26], and the method is easily applicable to a large range of porous systems. Future work could study, at the pore scale, a wide variety of single phase and multiphase flow in porous media problems at conditions representative of subsurface aquifers, oil and gas fields and other deep geological systems.

Disclosures

The authors have nothing to disclose.

Acknowledgements

We gratefully acknowledge funding from the Qatar Carbonates and Carbon Storage Research Centre (QCCSRC), provided jointly by Qatar Petroleum, Shell, and Qatar Science & Technology Park. We also acknowledge funding from the Imperial College Consortium on Pore-Scale Modelling.

References

1. *Special Report on Carbon Dioxide Capture and Storage.* Cambridge, U.K. (2005).
2. Ennis-King, J., & Paterson, L. Engineering aspects of geological sequestration of carbon dioxide. *SPE 77809, Proceedings of the Asia Pacific Oil and Gas Conference and Exhibition.* doi: 10.2523/77809-MS (2002).
3. Weir, G. J., White, S. P., & Kissling, W. M. Reservoir storage and containment of greenhouse gases. *Transport in Porous Media.* **23** (1), 61-82, doi: 10.1007/BF00145266 (1996).
4. Lindeberg, E., & Wessel-Berg, D. Vertical convection in an aquifer column under a gas cap of CO_2. *Energy Conversion & Management.* **38**, 229-234 (1997).
5. Lin, H., Fujii, T., Takisawa, R., Takahashi, T., & Hashida, T. Experimental evaluation of interactions in supercritical CO_2/water/rock minerals system under geologic CO_2 sequestration conditions. *Journal of Materials Science.* **43** (7), 2307-2315, doi: 10.1007/s10853-007-2029-4 (2007).
6. Juanes, R., Spiteri, E. J., Orr Jr., F. M., & Blunt, M. J. Impact of relative permeability hysteresis on geological CO_2 storage. *Water Resources Research.* **42** (12), doi: 10.1029/2005WR004806 (2006).
7. Hesse, M., Orr Jr., F. M., & Tchelepi, H. A. Gravity Currents with Residual trapping. *Journal of Fluid Mechanics.* **661**, 35-60, doi: 10.1017/SS002211200800219X (2008).
8. MacMinn, C., Szulczewski, M. L., & Juanes, R. CO_2 migration in saline aquifers. Part 1. Capillary trapping under slope and groundwater flow. *Journal of Fluid Mechanics.* **662**, 329-351, doi: 10.1017/S0022112010003319 (2010).
9. MacMinn, C., Szulczewski, M. L., & Juanes, R. CO_2 migration in saline aquifers. Part 2. Capillary and solubility trapping. *Journal of Fluid Mechanics.* **688**, 321-351, doi: 10.1017/jfm.2011.379 (2011).
10. Qi, R., LaForce, T. C., & Blunt, M. J. Design of carbon dioxide storage in aquifers. *International Journal of Greenhouse Gas Control.* **3** (2), 195-205, doi: 10.1016/j.ijggc.2008.08.004 (2009).
11. Flannery, B. P., Deckman, H. W., Roberge, W. G., & D'Amico, K. L. Three-Dimensional X-Ray Microtomography. *Science.* **237** (4821), 1439-1444, doi: 10.1126/science.237.4821.1439 (1987).
12. Jatsi, J. K., Jesion, G., & Feldkamp, L. Microscopic Imaging of Porous Media with X-Ray Computer Tomography. SPE 20495. *SPE Formation Evaluation.* 189-193, doi: 10.2118/20495-PA (1993).
13. Blunt, M. J. *et al.* Pore-scale imaging and modelling. *Advances in Water Resources.* **51**, 197-216, doi: 10.1016/j.advwatres.2012.03.003 (2013).
14. Cnudde, V., & Boone, M. N. High-resolution X-ray computed tomography in geosciences: A review of the current technology and applications. *Earth-Science Reviews.* **123**, 1-17, doi: 10.1016/j.earscirev.2013.04.003 (2013).
15. Wildenschild, D., & Sheppard, A. P. X-ray imaging and analysis techniques for quantifying pore-scale structure and processes in subsurface porous medium systems. *Advances in Water Resources.* **51**, 217-246, doi: 10.1016/j.advwatres.2012.07.018 (2013).
16. Espinoza, D. N., & Santamarina, J. C. Water-CO_2-mineral systems: Interfacial tension, contact angle, and diffusion-Implications to CO_2 geological storage. *Water Resources Research.* **46** (7), doi: 10.1029/2009WR008634 (2010).
17. Li, X., Boek, E., Maitland, G., & Trusler, J. P. M. Interfacial Tension of (Brines + CO_2): (0.864 NaCl+0.136 KCl) at Temperatures between (298 and 448) K, Pressures between (2 and 50) MPa, and Total Molalities of (1 to 5) mol/kg. *Journal of Chemical and Engineering Data.* **57** (4), 1078-1088, doi: 10.1021/je201062 (2012).
18. Spiteri, E. J., Juanes, R., Blunt, M. J., & Orr Jr., F. M. A New Model of Trapping and Relative Permeability Hysteresis for All Wettability Characteristics. *SPE Journal.* **13** (3), 277-288, doi: 10.2118/96448-PA (2008).
19. Chaudhary, K. *et al.* Pore-scale trapping of supercritical CO_2 and the role of grain wettability and shape. *Geophysical Research Letters.* **40**, 1-5, doi: 10.1002/grl.50658 (2013).
20. Karpyn, Z. T., Piri, M., & Singh, G. Experimental investigation of trapped oil clusters in a water-wet bead pack using X-ray microtomography. *Water Resources Research.* **46** (4), doi: 10.1029/2008WR007539 (2010).
21. Wildenschild, D., Armstrong, R. T., Herring, A. L., Young, I. M., & Carey, J. W. Exploring capillary trapping efficiency as a function of interfacial tension, viscosity, and flow rate. *Energy Procedia.* **4**, 4945-4952, doi: 10.1016/j.egypro.2011.02.464 (2011).

22. Silin, D., Tomutsa, L., Benson, S. M., & Patzek, T. W. Microtomography and Pore-Scale Modeling of Two-Phase Fluid Distribution. *Transport in Porous Media.* **86**, 495-515, doi: 10.1007/s11242-010-9636-2 (2011).
23. Andrew, M. G., Bijeljic, B., & Blunt, M. J. Pore-scale imaging of geological carbon dioxide storage under *in situ* conditions. *Geophysical Research Letters.* **40** (15), 3915-3918, doi: 10.1002/grl.50771 (2013).
24. Andrew, M. G., Bijeljic, B., & Blunt, M. J. Pore-scale imaging of trapped supercritical carbon dioxide in sandstones and carbonates. *International Journal of Greenhouse Gas Control.* **22**, 1-14, doi: 10.1016/j.ijggc.2013.12.018 (2014).
25. Hassler, G. L. Method and Apparatus for Permeability Measurements. *U.S.A. patent.* (1944).
26. Andrew, M. G., Bijeljic, B., & Blunt, M. J. Pore-scale contact angle measurements at reservoir conditions using X-Ray microtomography. *Advances in Water Resources.* **68**, 24-31, doi: 10.1016/j.advwatres.2014.02.014 (2014).
27. Iglauer, S., Paluszny, A., Pentland, C. H., & Blunt, M. J. Residual CO_2 imaged with x-ray micro-tomography. *Geophysical Research Letters.* **38**, doi: 10.1029/2011GL049680 (2011).
28. Carroll, J. J., Slupsky, J. D., & Mather, A. E. The Solubility of Carbon Dioxide in Water at Low Pressure. *Journal of Physical and Chemical Reference Data.* **20** (6) (1991).
29. Poludniowski, G. Calculation of x-ray spectra emerging from an x-ray tube. Part II. X-ray production and filtration in x-ray targets. *Medical Physics.* **34** (2175), doi: dx.doi.org/10.1118/1.2734726 (2007).
30. Poludniowski, G., & Evans, P. M. Calculation of x-ray spectra emerging from an x-ray tube. Part I. Electron penetration characteristics in x-ray targets. *Medical Physics.* **34** (2161), doi: dx.doi.org/10.1118/1.2734725 (2007).
31. Poludniowski, G., Landry, G., DeBlois, F., Evans, P. M., & Verhaegen, F. SpekCalc: a program to calculate photon spectra from tungsten anode x-ray tubes. *Physics in Medicine and Biology.* **57** (19), doi: 10.1088/0031-9155/54/19/N01 (2009).
32. Berger, M. J. *et al.XCOM: Photon Cross Section Database (version 1.5)*. National Institute of Standards and Technology, Gaithersburg, MD (2007).
33. Buades, A., Coll, B., & Morel, J.-M. A non-local algorithm for image denoising. *Computer Vision and Pattern Recognition.* doi: 10.1109/CVPR.2005.38 (2005).
34. Buades, A., Coll, B., & Morel, J.-M. Nonlocal Image and Movie Denoising. *International Journal of Computer Vision.* **76**(2), 123-139, doi: 10.1007/s11263-007-0052-1 (2008).
35. Schluter, S., Sheppard, A. P., Brown, K., & Wildenschild, D. Image processing of multiphase images obtained via X-ray microtomography: A review. *Water Resources Research.* **50** (4), 3615-3639, doi: 10.1002/2014WR015256 (2014).
36. Jones, A. C. *et al.* Assessment of bone ingrowth into porous biomaterials using MICRO-CT. *Imaging Techniques for Biomaterials Characterization.* **28** (15), 2491-2504, doi: 10.1016/j.biomaterials.2007.01.046 (2007).
37. Schneider, C. A., Rasband, W. S., & Eliceiri, K. W. NIH Image to ImageJ: 25 years of image analysis. *Nature Methods.* **9**, 671-675, doi: 10.1038/nmeth.2089 (2012).
38. El-Maghraby, R. *Measurements of CO_2 trapping in Carbonate and Sandstone Rocks.* Imperial College, London, (2013).
39. Roof, J. G. Snap-Off of Oil Droplets in Water-Wet Pores. *SPE Journal.* **10** (1), 85-90, doi: 10.2118/2504-PA (1970).
40. Lenormand, R., Zarcone, C., & Sarr, A. Mechanisms of the displacement of one fluid by another in a network of capillary ducts *Journal of Fluid Mechanics.* **135**, 337-353, doi: 10.1017/S0022112083003110 (1983).
41. Dias, M. M., & Wilkinson, D. Percolation with trapping. *Journal of Physics A: Mathematical and General.* **19**, 3131-3146, doi: 10.1088/0305-4470/19/15/034 (1986).
42. Fisher, M. E. The theory of equilibrium critical phenomena. *Reports on Progress in Physics.* **30** (2), 615, doi: 10.1088/0034-4885/30/2/306 (1967).
43. Lorenz, C. D., & Ziff, R. M. Precise determination of the bond percolation thresholds and finite-size scaling corrections for the sc, fcc and bcc lattices. *Physical Review E.* **57** (1), 230-236, doi: 10.1103/PhysRevE.57.230 (1998).
44. Levenberg, K. A method for the solution of certain non-linear problems in least squares. *Quarterly Journal of Applied Mathmatics.* **2**(2), 164-168 (1944).
45. Marquardt, D. W. An Algorithm for Least-Squares Estimation of Nonlinear Parameters. *Journal of the Society for Industrial and Applied Mathematics.* **11** (2), 431-441 (1963).
46. Holland, P. W., & Welsch, R. E. Robust regression using iteratively reweighted least-squares. *Communications in Statistics - Theory and Methods.* **6** (9), 813-827, doi: 10.1080/03610927708827533 (1977).
47. Huber, P. J. *Robust Statistics.* John Wiley & Sons, Inc., New York, NY (1981).
48. Akbarabadi, M., & Piri, M. Relative permeability hysteresis and capillary trapping characteristics of supercritical CO_2/brine systems: An experimental study at reservoir conditions. *Advances in Water Resources.* **52**, 190-206, doi: 10.1016/j.advwatres.2012.06.014 (2013).
49. Pentland, C. H., El-Maghraby, R., Iglauer, S., & Blunt, M. J. Measurements of the capillary trapping of super-critical carbon dioxide in Berea sandstone. *Geophysical Research Letters.* **38**, 4, doi: 10.1029/2011GL046683 (2011).
50. El-Maghraby, R. M., & Blunt, M. J. Residual CO_2 Trapping in Indiana Limestone. *Environmental Science and Technology.* **47**(1), 227-233, doi: 10.1021/es304166u (2013).
51. Sheppard, A. P., Sok, R. M., & Averdunk, H. Techniques for image enhancement and segmentation of tomographic images of porous materials. *Physica A.* **339** (1-2), 145-151, doi: 10.1016/j.physa.2004.03.057 (2004).